International Journal of Advanced Technology and Engineering Exploration, Vol 12(123)
ISSN (Print): 2394-5443 ISSN (Online): 2394-7454
http://dx.doi.org/10.19101/IJATEE.2024.111100612

Research Article

High-isolation dual-band slotted patch MIMO antenna for sub-6 GHz 5G applications

Kakade Sandeep[1*], Nirmal Sharma[2] and Navnath Narawade[3]
Research Scholar, Electronics and Communication Engineering, School of Engineering and Technology, Nirwan University, Jaipur, Rajasthan, India[1]
Professor, Electronics and Communication Engineering, School of Engineering and Technology, Nirwan University, Jaipur, Rajasthan, India[2]
Professor, Electronics and Communication Engineering, Parvatibai Genba Moze College of Engineering, Wagholi, Pune, Maharashtra, India[3]

Received: 23-April-2024; Revised: 25-February-2025; Accepted: 27-February-2025

Abstract
In this research, an extremely isolated dual-band multiple-input-multiple-output (MIMO) antenna for fifth-generation (5G) networks operating at sub-6 GHz is presented. The proposed antenna operates within the n77, n78, and n46 frequency bands, which are critical for 5G communication systems. To improve bandwidth and isolation, the patch structure is modified with a combination of rectangular and circular slots. To further minimize mutual coupling, a rectangular strip is placed between the radiating elements. The final design employs a triangular-shaped radiating element with perforations, which reduces surface current and increases bandwidth. The antenna, constructed using flame retardant 4 (FR4) materials, was tested to validate its functionality in anechoic chambers and with a vector network analyzer (VNA). The resonance frequencies of the antenna are 3.14 GHz and 5.42 GHz, with isolation values measured at -25 dB and -42.59 dB, respectively. The bandwidth achieved during testing was 2.26 GHz, making the antenna for C-band applications. The envelope correlation coefficient (ECC) was approximately 0.001, significantly lower than the maximum allowable value, ensuring optimal diversity performance. The conceived MIMO antenna showed low ECC, high isolation, and broad bandwidth, rendering it a viable option for 5G applications operating at sub-6 GHz. These outcomes make it an optimal fit for 5G applications, which achieve substantial isolation while maintaining a compact size.

Keywords
Multiple-input-multiple-output (MIMO), Sub-6 GHz 5G, High isolation, Dual-band operation, C-band applications, Mutual coupling reduction, 5G applications.

1.Introduction
The advent of fifth-generation (5G) technology marks a revolutionary shift in modern communication networks, highlighting the increasing demand for high-efficiency antennas, particularly in the sub-6 GHz range. With the global rollout of 5G, multiple-input-multiple-output (MIMO) systems have become indispensable for achieving higher data rates, greater capacity, and reduced latency. However, a significant challenge in MIMO antenna design lies in maintaining strong isolation between antenna components to minimize mutual coupling, which can degrade overall system performance [1].

Recent studies have demonstrated the effectiveness of defected ground structures (DGS) and slotted patch techniques in achieving high isolation in compact MIMO systems. Various research efforts have focused on improving antenna performance by employing slotting methods and advanced decoupling mechanisms [2]. Due to the miniaturization of radio frequency (RF) systems, compact antenna designs face increased mutual coupling, which affects radiation characteristics. To address this issue, researchers have explored diverse strategies, including decoupling techniques, artificial magnetic conductors (AMC), and metasurfaces, to enhance compactness and mitigate mutual coupling [3]. As RF systems continue to shrink, an increasing focus has been placed on designing compact antenna systems. Nevertheless, the miniaturization of antenna

*Author for correspondence

elements leads to intense mutual interaction, distorting radiation characteristics. Consequently, researchers have extensively explored strategies to enhance compactness and minimize mutual coupling among MIMO antenna elements [4]. These advancements establish a strong basis for developing compact and high-performance MIMO antennas with enhanced isolation, optimized for 5G networks operating at sub-6 GHz. Building on this foundation, the current study proposes a novel slotted patch antenna design that aims to achieve both high isolation and enhanced bandwidth, contributing to the evolving field of 5G antenna technology [5, 6]. MIMO antenna systems are integral to modern 5G networks, offering enhanced capacity, improved data rates, and robust reliability [7]. Data traffic generated by numerous social applications, video streaming, Internet of Things (IoT), cloud services, and related platforms is anticipated to surpass the capabilities of fourth-generation (4G) infrastructure [8]. Increased connectivity, lower latency, and reduced energy consumption will also be key characteristics of future communication technologies. While these aspects are crucial, 5G and the upcoming sixth-generation (6G) technologies offer significantly greater capabilities than 4G. The compact design of modern MIMO antennas usually leads to significant mutual coupling between antenna components, resulting in degraded performance. To address these challenges, innovative design strategies have been developed, including slotted antenna structures, DGS, and metasurfaces, which effectively reduce coupling and improve isolation. Additionally, advanced decoupling techniques and AMC have demonstrated substantial enhancements in antenna bandwidth and radiation characteristics [9, 10]. Among these, slotted patch antennas have been recognized as a highly efficient remedy for boosting isolation. By incorporating slots into the patch, these antennas achieve more impedance matching, wider bandwidth, and reduced interference between elements. Further improvements are achieved through the integration of decoupling structures and design modifications, which significantly minimize mutual coupling. These techniques are particularly crucial for 5G applications, where low latency, high data rates, and reliable connectivity are paramount [11, 12]. Ensuring both high isolation and compactness remains a significant challenge, especially in multi-port MIMO systems operating within the sub-6 GHz spectrum [13]. The close proximity of antenna elements in compact designs often leads to severe mutual coupling, which distorts radiation patterns and degrades overall system performance. This issue becomes even more critical in space-constrained environments such as smartphones, where high-performance antennas are essential. Effectively addressing these challenges necessitates innovative design strategies that optimize isolation, compactness, and wideband performance [14, 15].

The objective of this study is to design and develop a slotted patch MIMO antenna that effectively minimizes mutual coupling and overcomes bandwidth limitations in compact 5G antenna systems. By leveraging slotting techniques and optimized layouts, this work aims to enhance isolation and support wideband operation within the sub-6 GHz spectrum.

The paper is structured as follows: Section 2 reviews advancements in MIMO antenna design, focusing on isolation and bandwidth enhancements. Section 3 details the design methodology and simulation of the proposed slotted patch antenna. Section 4 presents simulation and experimental results, highlighting key performance metrics. Section 5 compares findings with previous designs, while Section 6 concludes with insights and recommendations for future research.

2.Literature review

An extensive review of available literature shows that many researchers have worked on optimal and efficient designs for various applications with the incorporation of MIMO systems. The modeling and analysis of a multiband rectangular microstrip antenna for 5G applications were discussed. The antenna, made of RT/Duroid 5880 substrate, exhibited low voltage standing wave ratio (VSWR) values, and at frequencies between 3.5 GHz and 11.65 GHz, 99.98% of the forward power is available, making it suitable for 5G applications [16]. This study proposes a method to improve isolation between large MIMO antenna parts, particularly for 5G applications. The design uses flame retardant 4 (FR4) materials, which improves mutual coupling, bandwidth, and gain. The proposed design suppresses mutual coupling, increases bandwidth, and improves the envelope correlation coefficient (ECC), thereby enhancing antenna performance for 5G C-band applications [17]. A MIMO antenna system for 5G communications consists of a microstrip feed into a square patch. The metasurface layer enhances isolation between components and increases gain. The system attains an extensive bandwidth of 4.56 GHz, a maximum gain of 8.3 dBi, and outstanding isolation. It also has high overall efficiency (82%)

and a small inter-element distance of 22 mm. The metasurface layer boosts gain and isolation; it offers a viable alternative for next-generation wireless communication applications [18]. They proposed a compact MIMO antenna using circular ring slot radiators and complementary split-ring resonators (CSRRs) for 5G applications. With high isolation (>20 dB), a narrow ECC (<0.005), and high radiation efficiency (~80%), it supports dual-polarized operation in the 3.4–3.8 GHz range. The design optimizes space and enhances diversity performance, achieving low channel capacity loss (CCL) (<0.4 b/s/Hz). The CSRRs reduce mutual coupling between ports, confirming suitability for high-data-rate 5G networks [19]. A high-performance 5G antenna array on an RT-Duroid 5880 substrate features a circular microstrip patch with MIMO feeding, optimized for operation at 35 GHz. It confers a gain of 8.8 dB and an excellent S11 value of -41.9 dB, with simulations indicating its superiority over single-element and 2×2 rectangular microstrip patch antenna designs [20], a compact 5G MIMO antenna designed for automobile communication, operates at 1.9 GHz and 5.9 GHz, offering ECC values below 0.3 and a diversity gain (DG) of 10 dB. Its reduced size and improved performance make it ideal for vehicle communication systems [21]. Additionally, a MIMO antenna with two elements, operating at 29 GHz, includes slits in its radiators, enabling a compact design of 11.4 × 5.3 mm^2. It demonstrates low mutual coupling, an ECC of 0.001, and a DG exceeding 9.8 dB, making it suitable for advanced 5G communication [22]. A millimeter-wave microstrip array antenna designed for 5G networks, featuring a DGS to decrease mutual coupling and increase gain was introduced. Built on a Rogers RT-5880 substrate, the design achieves compact dimensions of 6 mm × 6 mm for a single element and 9 mm × 13 mm for a two-element array. Operating at 39.96 GHz, it delivers gains of 6.4 dBi (single element) and 11.6 dBi (two-element array) with bandwidths of 2.3 GHz and 2.1 GHz and efficiencies of 73.5% and 85%, respectively. Optimized using computer simulation technology (CST), the antenna demonstrates a stable directional radiation pattern, making it ideal for licensed 5G applications across various countries [23]. The research investigated a compact MIMO antenna designed for dual-band operation supporting long term evolution (LTE), 4G, and 5G networks. The antenna, featuring an F-typed radiator with a rectangular ground plane and a circular slot, operates in the frequency ranges of 1.8– 2.3 GHz and 3.7– 4.2 GHz with resonances at 1.8 GHz and 3.9 GHz. Structured on an FR-4 substrate with dimensions of 48 × 48 mm^2, the antenna achieves outstanding diversity performance, as demonstrated by a low ECC (< 0.002), high DG (> 9.9 dB), and low total active reflection coefficient (TARC) (< -25 dB). Results from measurements and simulations indicate good agreement, and the omnidirectional radiation patterns and compact design make this antenna well-suited for next-generation wireless [24]. The CST simulator is used to study a multi-element MIMO antenna with an inverted T-shaped ground structure and two symmetrical hexagon-shaped radiators. The analysis focuses on several aspects, including radiation patterns, effective gain, S-parameters, and current distribution. With an efficiency of 88% and a gain of more than 4.5 dB, the antenna shows a significant association between the measured and simulated data [25]. The design incorporates four radiating elements shaped like spanners, arranged in a radial pattern on a FR4 substrate. The tapered feeding lines enable simultaneous operation in two frequency bands. The design achieves minimal mutual coupling and low ECC while also providing excellent gain and efficiency. The comparative study highlights this product's advantages in terms of its applicability, performance, and size [26]. This paper presented a miniature two-element wideband MIMO antenna optimized for Sub-6 GHz applications, specifically targeting the n77, n78, and n79 bands. The antenna, with measurements of 36×18×1.6 mm^3, employs symmetrical circular slot monopoles and a T-shaped ground stub to enhance isolation. The design achieved an isolation of -30 dB, a reflection coefficient (S11) below -15 dB, and an operational bandwidth spanning 3.2 to 5.75 GHz, making it highly effective [27]. This article presents a dual-band antenna optimized for WiMAX and 5G applications. The design operates within the frequency bands of 2–3.71 GHz and 5.9–7.54 GHz, covering essential WiMAX and 5G sub-6-7 GHz bands. The antenna features tiny dimensions of 63 × 50 mm^2, achieving a maximal gain of 6.47 dBi, while the MIMO configuration shows a peak gain of 7.5 dBi. Notably, this MIMO system exhibits impressive performance, including low ECC (< 0.0002), minimal CCL, and excellent radiation efficiency. Consequently, it is perfect for modern wireless communication systems [28]. With two rectangular-shaped patches linked by a corporate feed network and two quarter-wavelength square CSRRs on the ground plane, the antenna is compact, flat, and effective. Utilizing 5G frequency bands, this technology provides a bandwidth of 3.9 GHz, reaching a maximum gain of 11 dBi and a radiation efficiency of more than 95% at 28 GHz. The antenna's exceptional diversity performance is confirmed by a range of performance measurements. Utilizing CSRR and DGS improves the amplification, frequency range, and separation, rendering it appropriate for 5G applications [29]. In this study, a compact four-element antenna for 5G communications aimed at the new radio (NR) n77 and n78 channels is introduced. The 40×40×1.6 mm^3 antenna is created in high frequency structure simulator (HFSS) software and manufactured on FR4. An "EH" slot and protruded stubs improve bandwidth and impedance matching, outperforming 5G antennas with low ECC and a DG near 10 dB [30]. The study emphasizes the significance of MIMO antennas in 5G wireless communication systems. It introduces a compact, efficient 1×2 MIMO antenna design for the 5 to 7 GHz frequency range, commonly used in IoT applications. The design uses copper materials on an FR4 substrate and incorporates a feeding network to improve signal strength. The design meets wireless communication requirements, and simulations show optimized performance in two-element MIMO antennas, indicating potential for further application in IoT and mobile communications devices [31]. In this paper, the author presented a compact 2 × 1 ultra-wideband (UWB) MIMO antenna, measuring 40 × 20 × 1.6 mm^3, designed for RF energy harvesting. The innovative use of four "A"-shaped slots improved isolation and impedance matching, enabling a wide operational bandwidth from 3.1 to 10.6 GHz. The antenna achieved remarkable performance, including a reflection coefficient below -20 dB and an ECC under 0.005, making it highly effective for UWB energy harvesting and wireless communication applications [32]. A flexible MIMO antenna made from jeans material for wearable use was used. It achieves an impedance bandwidth of 4.24–5.38 GHz with high isolation of 27.8 dB between ports. Design features like Y-shaped decoupling and shorting pins minimize mutual coupling, while specific absorption rate (SAR) analysis confirms safe wearable application suitability [33]. MIMO applications use a compact, dual-polarized, wideband antenna. Parasitic resonators, cross magnetic dipoles, and a wideband hybrid ring coupler are used. Low mutual coupling and ECC and a good front-back ratio characterize the antenna. Despite its compact size and high Q-factor-backed cavity constraints, it is appropriate for MIMO usage [34].

Overall, the review study highlighted significant advancements in MIMO antenna design for 5G applications, emphasizing techniques to improve isolation, bandwidth, and gain. Various approaches, including the use of metasurfaces, CSRRs, and DGS, have been explored to enhance performance. The findings suggest that compact MIMO antennas with optimized isolation and diversity characteristics are essential for next-generation wireless communication systems. Additionally, the study highlights the growing importance of dual-band and multi-band designs in addressing the increasing demands of 5G networks, particularly in the Sub-6 GHz and millimeter-wave spectrum.

3.Methodology

HFSS is a software application used for designing MIMO antennas and performing three-dimensional electromagnetic modeling. The design and simulation are performed using HFSS, an ideal tool for modeling complex antenna configurations. Using this 3D modeler, the antenna is designed according to the geometrical parameters obtained theoretically. The radiation boundary is applied to emulate free-space conditions, and a microstrip feeding mechanism is used, with separate wave ports assigned to each input. HFSS employs the finite element method, and automatic meshing is selected before starting the simulation. After post-processing, HFSS provides various parameters such as S11, S12, VSWR, radiation patterns, ECC, DG, etc. HFSS’s powerful simulation tools and post-processing capabilities make it an ideal tool for developing and refining MIMO antenna designs. When designing the antenna, one must consider the expected frequency range, the number of antenna elements required, bandwidth requirements, and the desired level of isolation. Begin by placing each component on the chosen substrate material, and then refine the design to meet the specified bandwidth requirements.

3.1Design of single reference antenna

The MIMO antenna employs an FR4 substrate with a thickness of 1.6 mm, designed as a single unit. A square patch design was selected due to its simplicity and ease of fabrication. This design is expected to exhibit a broadside radiation pattern and operate within a single frequency band, based on the patch's measurements. Maxwell's equations are used to calculate the geometrical parameters of the patch, substrate, ground plane, and feed line, which serve as the foundation of developing a basic patch antenna. For this design, the substrate is made from FR4 material with a dielectric constant of 4.4 and a thickness of 1.6 mm. The proposed antenna works at a resonance frequency of 4.62 GHz. Geometric parameters of the patch antenna are evaluated using standard formulas, with Equation 1 employed to calculate the width of the patch.

$$Wp = \frac{c}{2f_r\sqrt{\frac{(\varepsilon_r+1)}{2}}} \quad (1)$$

Here, W_p stands for the patch width, c for the speed of light, which is 3×10^8 m/s, F_r for the resonance frequency, and εr for the value of the dielectric constant. The patch's length can be found using this Equation 2; it calculates the patch's physical length L_p by adjusting the effective length L_{peff} with the extension length ΔL_p due to fringing effects. In MIMO antennas, accurate patch length calculation is critical as it directly affects the resonant frequency and, thus, the antenna's operational frequency band.

$$L_p = L_{peff} - 2\Delta L_p \quad (2)$$

In this case, the patch's effective length is indicated by L_{peff}, while its extension length is indicated by ΔL_p. These values are derived using specific equations. The Equation 3 takes into account the operating frequency, the effective relative permittivity ε_{reff}, and the speed of light (c) to enhance the antenna's functionality and efficiency. The effective length L_{peff} is influenced by the dielectric constant and the speed of light c. It is adjusted to account for the change in electrical length due to the substrate's dielectric properties, which is essential for precise frequency tuning in the MIMO system.

$$L_{peff} = \frac{c}{2f_r\sqrt{\varepsilon_{reff}}} \quad (3)$$

$$\Delta L_p = 0.412h\frac{(\varepsilon_{reff}+0.3)(\frac{wp}{h}+0.264)}{(\varepsilon_{reff}-0.258)(\frac{wp}{h}+0.8)} \quad (4)$$

Equation 4 calculates the extension length ΔL_p, using the constant 0.412 to estimate the fringing effect based on the patch width-to-height ratio. For MIMO antennas, reducing fringing losses is important to maintain consistent performance and isolation between elements.

The effective dielectric constant, represented by the symbol ε_{reff}, is calculated in Equation 5 by incorporating the patch dimensions and substrate thickness h. This effective dielectric constant affects the wavelength within the substrate, influencing both the resonant frequency and impedance matching, which are crucial for MIMO antenna efficiency.

$$\varepsilon_{reff} = \frac{\varepsilon_r+1}{2} + \frac{\varepsilon_r-1}{2}(1+12\frac{h}{w_p})^{-\frac{1}{2}} \quad (5)$$

Equation 6 provides an approximation of the substrate's length and width. It approximates the substrate length L_s by adding a multiple of the substrate thickness to the patch length. Proper substrate dimensions help in ensuring effective radiation patterns and minimizing mutual coupling between MIMO elements.

$$L_s = 6h + L_p \quad (6)$$

Equation 7 calculates the substrate width w_s by adding a multiple of the substrate thickness to the patch width. In MIMO designs, substrate width must be optimized to balance compactness and isolation, enhancing the system's performance in high-density antenna configurations.

$$W_s = 6h + W_p \quad (7)$$

To achieve the desired results, the acquired values are carefully adjusted. A patch antenna with overall dimensions of 26 × 26 mm² and an emitting element measuring 16 × 18 mm² is designed, as shown in *Figure 1*. The measurements of the reference antenna are L_s = 26 mm, Ws = 26 mm, L_p = 18 mm, W_p= 16 mm, L_f= 1 mm, and W_f = 5 mm. A 50-ohm sub-miniature version A (SMA) connector, made from materials such as perfect electric conductor (PEC) and Teflon with relative permittivity values of 1 and 2.1, respectively, is employed to connect the antenna. The simulation software exhibited superior performance compared to traditional wave port designs.

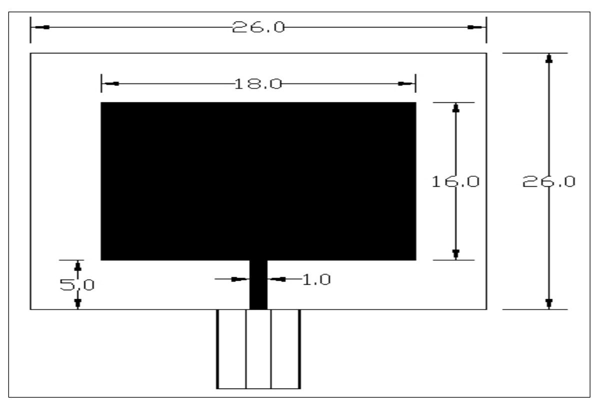

Figure 1 Single antenna shown geometrically (Antenna 1)

Using HFSS, the return loss of this design at 4.28 GHz is calculated to be -10.42 dB, with a VSWR of 1.86. Further modifications were made to the design by incorporating circular slots with a diameter of 4 mm and rectangular slots measuring 4 mm × 8 mm, each with a width of 1 mm, on the radiating element.

Additionally, DGS with slots measuring 7 mm × 3 mm and 18 mm × 3 mm were implemented in the ground, as shown in *Figure 2*.

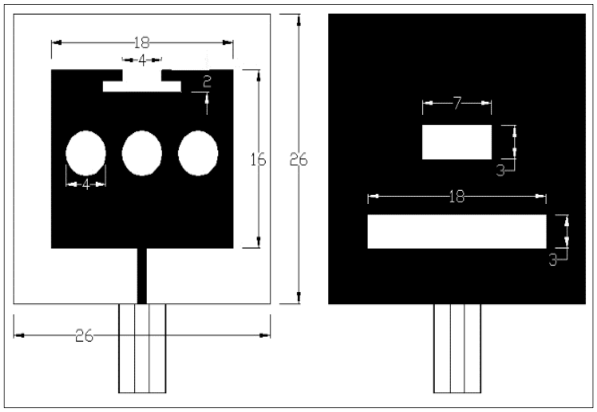

Figure 2 Modified design of single antenna (Antenna 2) (a) front and (b) back view

To modify the current distribution and, consequently, the resonant frequency and bandwidth, slots are often incorporated into antenna designs. Circular slots, in particular, are effective in enabling dual- or multi-frequency operation, allowing the antenna to function across multiple bands. The inclusion of slots in this design likely facilitates size reduction of the antenna without compromising its bandwidth or resonant frequency. Moreover, it helps in minimizing the patch size while maintaining performance. The specifications for this design include a VSWR of 1.06, a bandwidth of 0.76 GHz, a return loss of -29.85 dB, and a resonant frequency of 3.629 GHz. When circular and rectangular slots were introduced, the working frequency changed from 4.29 GHz to 3.6 GHz. A comparison of the return loss and VSWR is shown in *Figure 3*.

The design was further modified to attain a size reduction of up to 57% by employing a partial ground plane, as shown in *Figure 4*. This modification resulted in a resonant frequency of 3.663 GHz and a notable improvement in bandwidth from 0.76 GHz to 3.320 GHz. The shape of the radiating element was altered from a rectangle to a triangle. Additionally, punch holes were introduced along the edges of the patch element to reduce surface currents, as seen in *Figure 5*. Consequently, the radiating area of the antenna was reduced, contributing to a broader operating bandwidth. This improvement is evident in the plot shown in *Figure 6*. A return loss of -15.25 dB was achieved at 3.663 GHz, along with an enhanced bandwidth of 3.11 GHz.

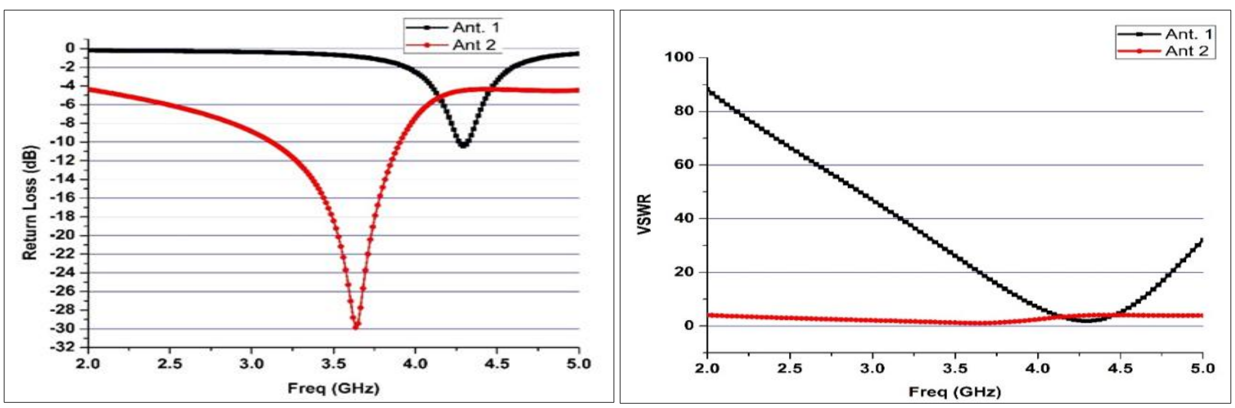

(a) (b)

Figure 3 Antenna 1 and 2's (a) Return loss and (b) VSWR

For the design, FR4 (1.6 mm) was chosen due to its low cost and availability, despite its moderate dielectric constant. Teflon was selected for its low signal loss and minimal dielectric constant, which improves bandwidth and efficiency. To simulate an ideal conductor and test maximum efficiency and radiation characteristics, PEC was used in the simulations. These materials strike a balance between cost, performance, and theoretical optimization. This work's main objective is to create a MIMO antenna that can cover the C-Band. Consequently, the initial stage in designing the proposed MIMO antenna is to arrange the individual antennas in an inverted configuration. The basic mode, or initial design, of the recommended MIMO antenna is shown in *Figure 7*. The two separate terminals of the MIMO antenna are clearly visible. It utilizes microstrip radiators with slots beneath the radiators and feed lines shaped like squares with cut corners, along with a lowered ground plane at the feed line's termination. To enhance element isolation, a rectangular strip of material measuring 18 mm by 3 mm was placed at the center. The distance between the centers of each antenna is 43.00 mm to ensure the critical spacing between the radiating elements. Antenna 1 demonstrates excellent performance, with a return loss of nearly -30 dB around 3.5 GHz and a wide VSWR bandwidth of less than 2: 1. Antenna 2 shows moderate performance, with a return loss around -7 dB and a VSWR near 1: 1 at 3.5 GHz, but with a narrower bandwidth compared to Antenna 1. Antenna 3 performs well across the 3–4.5 GHz range, with a return loss below -10 dB and a VSWR below 2: 1, indicating good impedance matching. Antenna 4 offers similar performance to Antenna 3, operating in the 2.7– 4.5 GHz range with acceptable return loss and VSWR values below 2: 1.

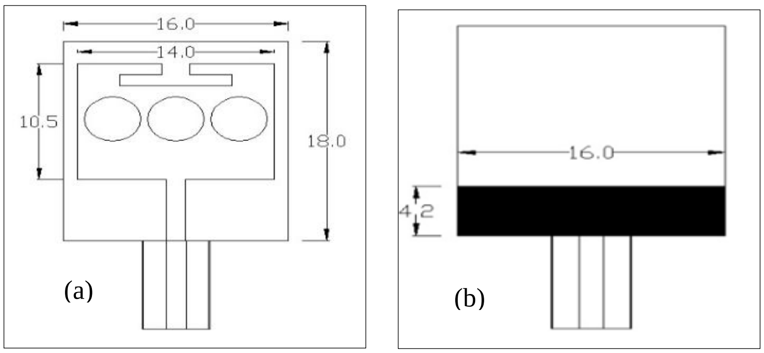

Figure 4 Reduced ground –antenna 3 (a) Front and (b) Back view

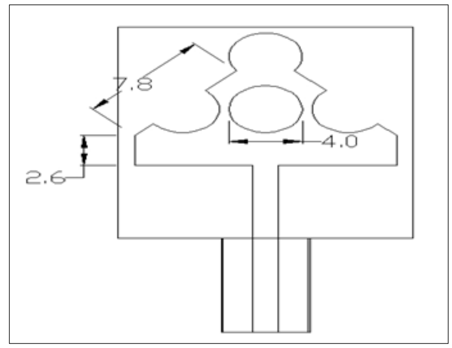

Figure 5 Antenna 4 is a triangle antenna with reduced ground and punch holes, like antenna 3

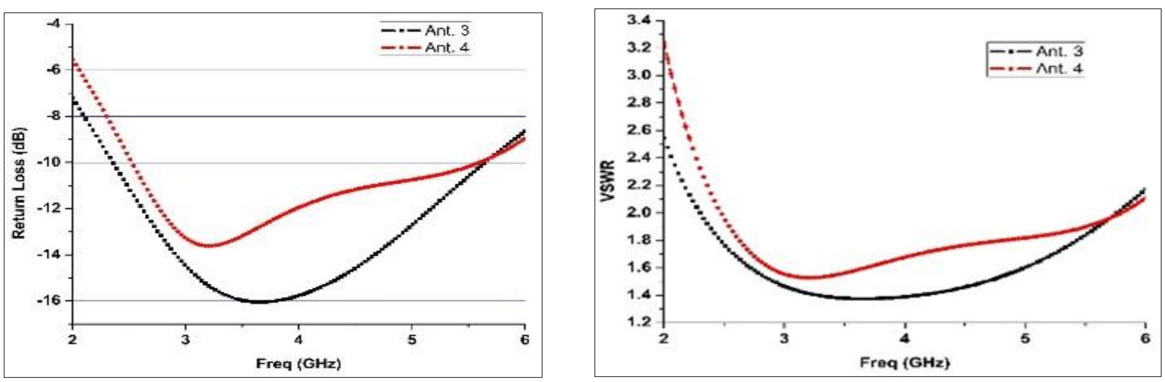

(a) (b)

Figure 6 Simulation results of antenna 3 and 4 (a) Return loss (b) VSWR

3.2MIMO antenna geometry

Appropriate spacing between antenna elements is critical to MIMO system performance. Achieving equilibrium between limiting mutual coupling and optimizing variety and capacity can be facilitated by adhering to the $\lambda/2$ spacing rule.

Using the parametric values provided in *Table 1*, two-element MIMO antennas were designed and simulated on the HFSS platform. The 2-element MIMO antenna is meticulously designed to be compact, measuring 59 mm × 20 mm in total dimensions. Each radiating element features a distinctive structure, incorporating a circular segment at the top with a diameter of 4 mm, situated 7.8 mm above the base, and a narrower section below with a width of 2.6 mm. The ground plane is optimized to 16 mm × 4.2 mm and includes 0.2 mm slits positioned 7.1 mm from the edges to enhance performance. To further improve functionality, a slot measuring 3.0 mm × 18 mm is introduced between the radiating elements, along with an additional ground section of 12 mm × 10.5 mm featuring rounded corners to boost signal isolation. A 3 mm gap separates the two radiating elements, minimizing interference and ensuring efficient operation. The design has shown promising results, which are discussed in the following section. The antenna was fabricated (*Figure 8*), and its radiation effectiveness was verified in an anechoic chamber, as well as through testing with a vector network analyzer (VNA) (Agilent N5247A).

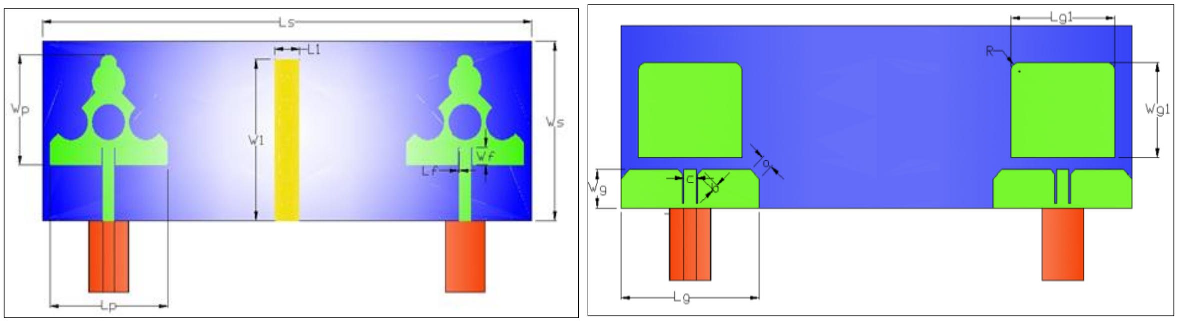

(a) (b)

Figure 7 Two element MIMO antenna configuration (a) front, (b) back profile

Table 1 Specifications for the anticipated dual-element antenna

Parameter	Value(mm)	Parameter	Value(mm)
L_s	59	W_s	20
a	1.41	b	0.71
L_p	14.2	W_p	12.3
L_{g1}	12	W_{g1}	10.5
c	1.4	d	0.2
L_g	16.	W_g	4.2
L_1	3	W_1	18

Minor inconsistencies in materials or manufacturing processes often cause differences between simulated and real-world performance in return loss or radiation patterns. The quality of the copper cladding and surface finish directly impacts surface current distribution and RF losses. Fabrication flaws or improper surface finishing introduce additional losses in the antenna design. To ensure the antenna performs as intended in simulations, designers carefully select the substrate, position the connector precisely, isolate the components effectively, and adhere strictly to manufacturing tolerances.

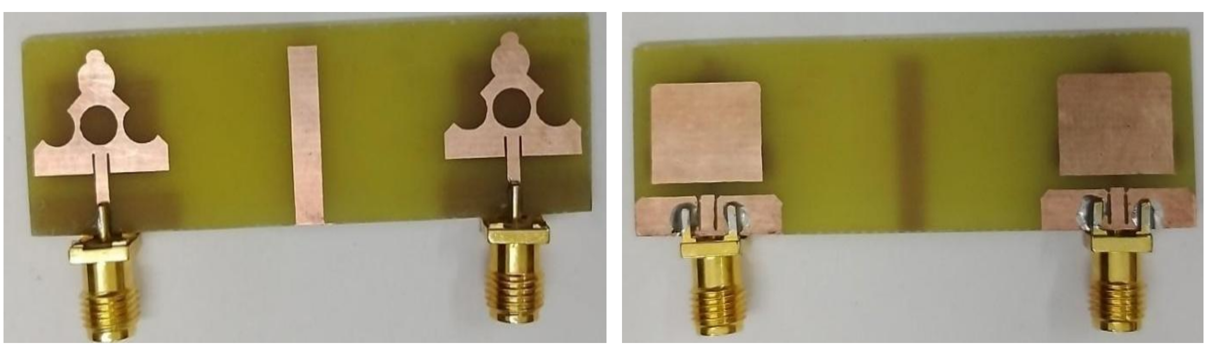

(a) (a)

Figure 8 Antenna fabrications (a) Front and (b) Back perspectives

4.Results

The validation process involves rigorous testing using equipment such as a VNA and an anechoic chamber with a standard reference horn antenna (*Figure 9*). The anechoic chamber provides an environment free from reflections. It is helpful for accurately evaluating an antenna's radiation characteristics, such as gain, efficiency, and radiation pattern. The rotating platform aligns the antenna for azimuth and elevation adjustments, while a standard horn antenna receives signals to analyze radiation performance. The measured results—including return loss, VSWR, radiation patterns, isolation, and gain—are compared with the simulated data.

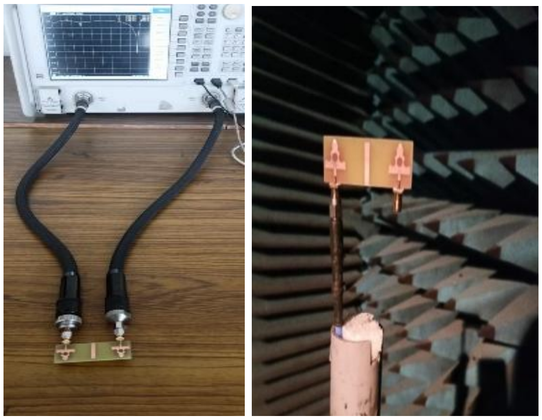

(a) (b)

Figure 9 Test setup of the prototype with (a) VNA and (b) anechoic chamber

4.1Reflection coefficients and isolation

The antenna ports are connected to a VNA to measure S11 (return loss), which evaluates impedance matching, typically at 50 ohms. A lower S11 value indicates better impedance matching and minimal signal reflection. During simulation, the designed MIMO antenna resonates at two frequencies: 3.28 GHz and 5.4 GHz. The maximum reflection coefficients observed are −29.12 dB and −15.32 dB (*Figure 10*), while the isolation values are −42.58 dB and −30.23 dB (*Figure 11*).

In experimental testing, the measured S-parameters, S11 and S22, are −11.25 dB at 3.02 GHz and −17.21 dB at 3.14 GHz, respectively. At higher frequencies, S11 and S22 values of −13.50 dB at 5.42 GHz and −19.42 dB at 5.5 GHz are obtained (*Figure 12*). The strong correlation between simulated and measured results confirms that the fabricated antenna closely adheres to the expected design, ensuring effective impedance matching for both ports.

The two-element MIMO antenna exhibits dual-band operation, covering 2.75 GHz to 4.63 GHz and 5.25 GHz to 5.53 GHz in simulations. The isolation levels are −30.55 dB and −42.59 dB (simulated) and −25.80 dB and −39.30 dB (measured) (*Figure 13*). Additionally, the measured bandwidth during testing is 2.26 GHz, effectively covering the n46, n77, and n78 frequency bands. The overall bandwidth achieved by this system is 2.26 GHz. Although minor deviations are observed at higher frequencies, the measured isolation values (S12 and S21) remain below -15 dB, ensuring sufficient isolation between antenna elements. Maintaining adequate port-to-port isolation is essential for minimizing mutual coupling in MIMO systems, as demonstrated by the constructed antenna. A good reflection coefficient (< -10 dB) confirms efficient operation within the designated frequency bands. Additionally, high isolation (> -15 dB) reduces interference between MIMO elements, enabling enhanced data rates and improved signal reliability.

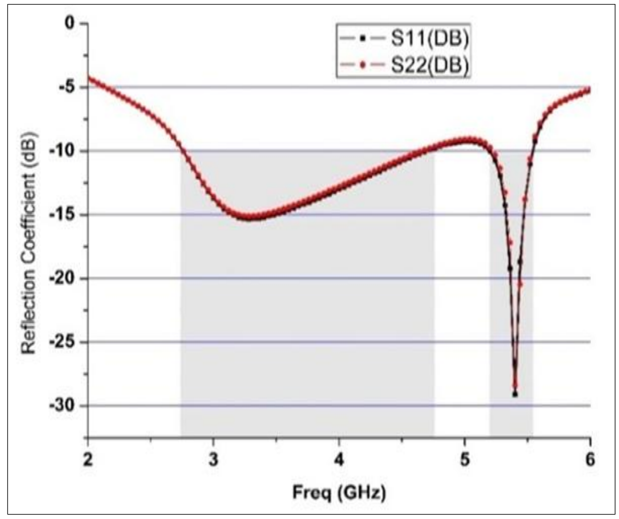

Figure 10 Simulated S11 and S22

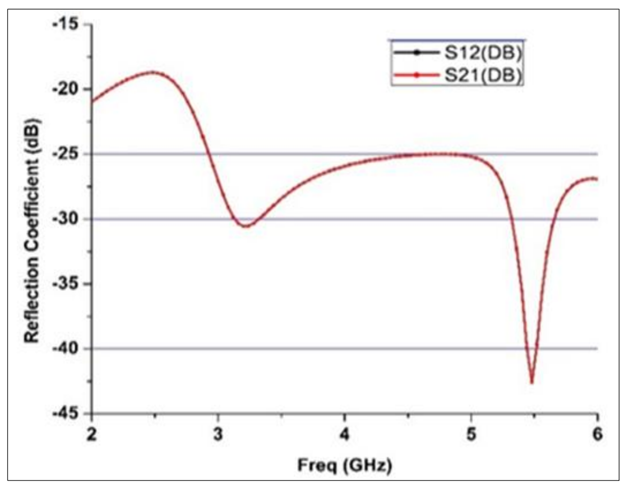

Figure 11 Simulated S12 and S21

4.2Radiation patterns

A controlled environment that mimics free-space conditions is created by removing reflections from the floor, ceiling, and walls using an anechoic chamber. This guarantees the measurement of only the antenna's direct radiation. On a turntable, the MIMO antenna is being tested. Usually rotating in azimuth and elevation, the antenna position is modified to ensure correct orientation with respect to the measuring system. Placed at a specified distance from the MIMO antenna is a calibrated receiving horn antenna. A single MIMO antenna port is stimulated at a time during radiation pattern measurement. Usually, 50 ohms is used to terminate the other port with a matched load in order to avoid interference with the measurement. *Figure 14* illustrates the simulated E-plane and H-plane radiation patterns of the two-port MIMO antenna at operating frequencies of 3.5 GHz and 5.4 GHz. The results indicate a well-defined directional action in both the E-plane and H-plane, demonstrating the antenna's suitability for dual-band applications. *Figure 15* presents the measured E-plane and H-plane patterns at the same frequencies, highlighting a good agreement with the simulated results. While slight discrepancies are observed, which may be attributed to fabrication tolerances and environmental factors during testing, the overall consistency verifies the antenna's design performance.

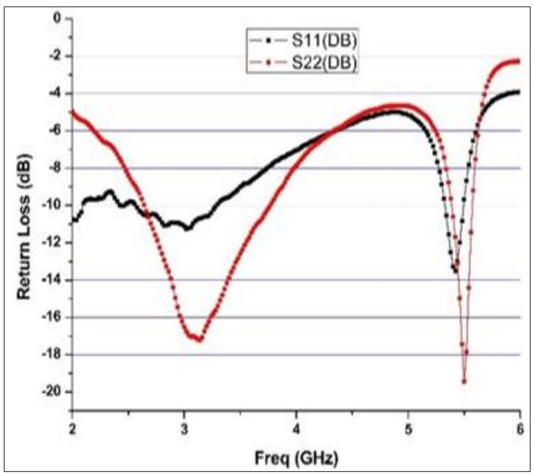

Figure 12 Measured S11 and S22

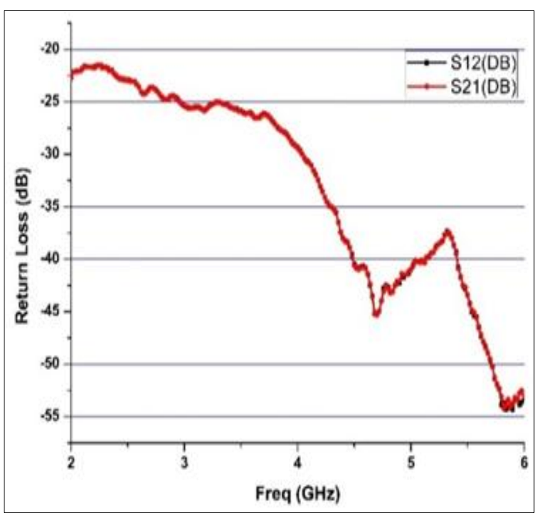

Figure 13 Measured S12 and S21

4.3Diversity performance

Diversity performance indicators are essential when analyzing the functionality of a MIMO antenna. To ensure optimal antenna evaluation, it is critical to assess parameters such as DG and ECC with the highest accuracy. Additionally, other important MIMO antenna metrics include DG, mean effective gain (MEG), CCL, and TARC, which collectively provide a comprehensive understanding of the antenna's performance as per Equation 8.

$$ECC = \frac{|S_{ij}^* S_{ij} + S_{ij}^* S_{jj}|^2}{(1-|S_{ii}|^2-|S_{ji}|^2)\left(1-|S_{jj}|^2-|S_{ij}|^2\right)} \quad (8)$$

Where the transmission coefficients are S_{ij} and S_{ji} and the reflection coefficients are S_{ii} and S_{jj}. It has been observed that the ECC is approximately equal to 0.001, which is quite smaller than the maximum allowable value for a MIMO antenna. It is a prerequisite for a MIMO antenna to have a TARC less than 0 dB. *Figure 16* presents the ECC plot. In MIMO systems, DG is closely related to ECC. The two metrics are often used together to assess the effectiveness of antenna systems in terms of signal quality and reliability. A DG higher than 9.99 dB implies that the ECC is extremely low, as shown in *Figure 17*. When it comes to strengthening signal resilience and facilitating communication in difficult settings, DG is essential as shown in Equation 9. Increased DG contributes to robust and dependable communication even in the face of fading signals.

$$DG = 10\sqrt{1 - ECC^2} \quad (9)$$

An additional metric called TARC is used to define the diversity efficacy of MIMO designs. The TARC is computed using the antenna system's S-parameters. These parameters indicate the properties of reflection and transmission between the ports. Equation 10 calculates the power reflected back at the antenna ports when both ports are excited simultaneously, accounting for the cumulative effects of the S-parameters. When multiple antennas are active, TARC measures how well the system radiates power. A low TARC value indicates that the MIMO system is well-matched with minimal mutual coupling, resulting in higher overall efficiency. For MIMO operation, the TARC value should be less than 0 dB. In the recommended MIMO antenna design, the TARC is −40 dB during simulation and testing (*Figure 18*), meeting the condition for efficient MIMO operation.

$$TARC = \sqrt{\frac{(S_{11}+S_{12})^2+(S_{22}+S_{21})^2}{2}} \quad (10)$$

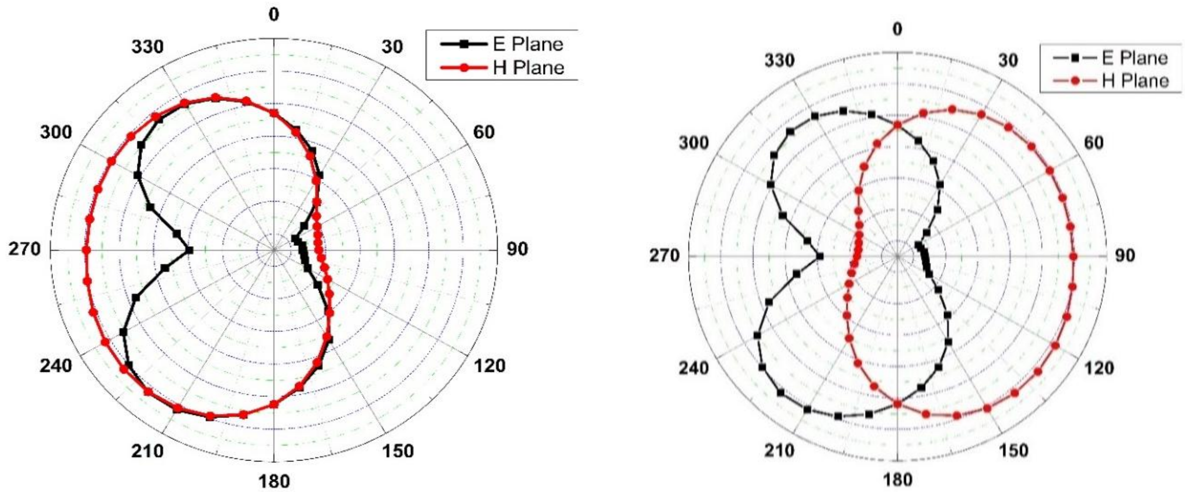

(a) (b)

Figure 14 Simulated E and H plane patterns at (a) 3.5 GHz and (b) 5.4 GHz

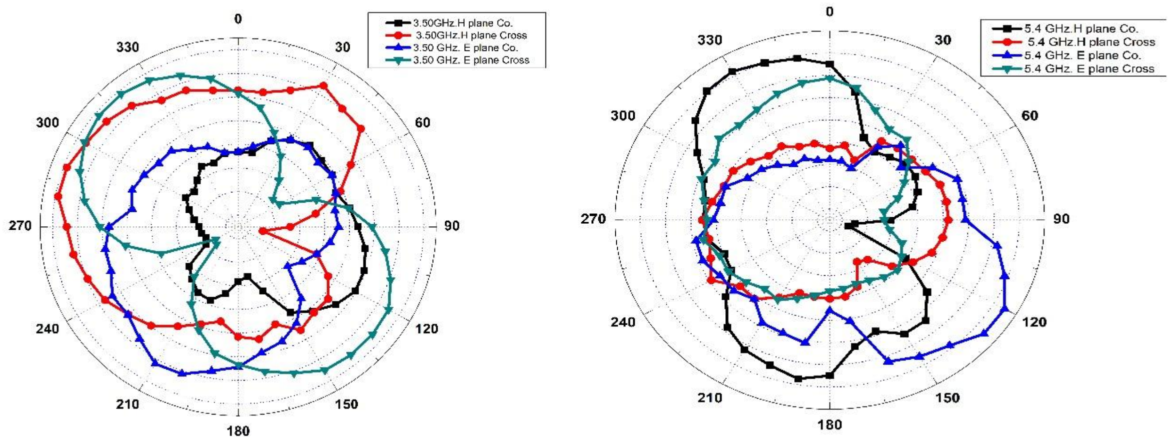

(a) (b)

Figure 15 Measured E and H plane patterns at (a) 3.5 GHz and (b) 5.4 GHz

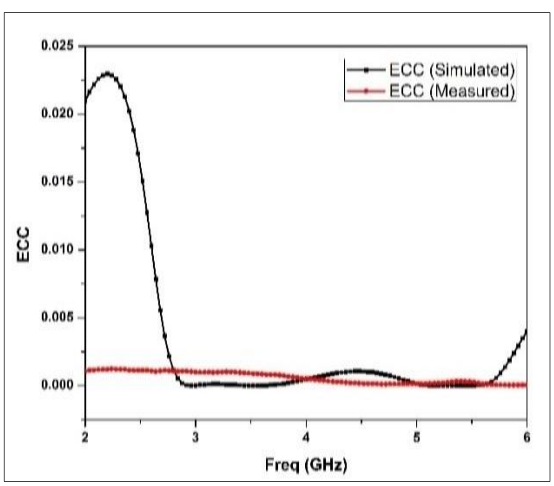

Figure 16 Simulated and measured ECC Values

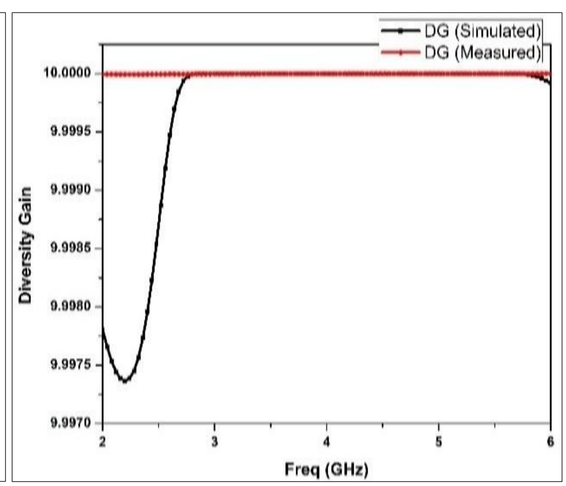

Figure 17 Simulated and measured DG

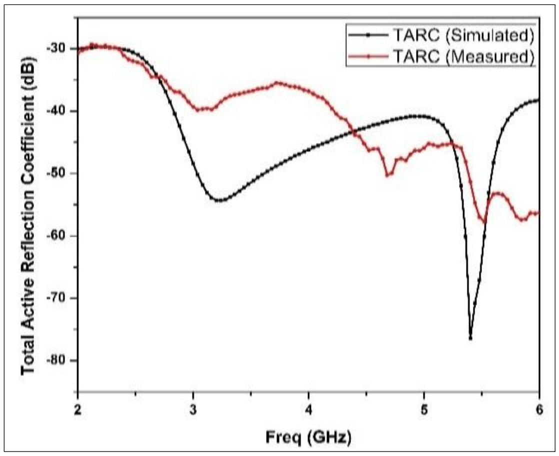

Figure 18 Simulated and measured TARC

CCL measures how effectively signals or information can be transmitted through a communication channel with minimal loss or interference. To ensure that MIMO systems can transmit and receive independent data streams, both ECC and CCL evaluate the correlation between signals from different antenna elements. Low ECC and low CCL lead to higher data rates and better spectrum utilization. CCL can be calculated using Equations 11, 12, and 13.

$$CCL = -log_2\, det(a) \quad (11)$$

a is the correlation matrix in this case.

$$a^R = \begin{pmatrix} \rho_{11} & \rho_{12} \\ \rho_{21} & \rho_{22} \end{pmatrix} \quad (12)$$

$$\rho_{ii} = 1 - \left(|S_{ii}|^2 + |S_{ij}|^2\right), and \quad (13)$$

$$\rho_{ij} = -\left(s_{ii} * s_{ij} + s_{ij} * s_{jj}\right),$$

$$for\ \ i\ and\ j =\ 1\ and\ 2$$

Table 2 provides a comprehensive comparison of simulated and measured results for the 2-port MIMO antenna, highlighting a strong correlation across key performance metrics, including impedance bandwidth, ECC, TARC, DG, isolation, and gain. The close agreement between these values confirms the antenna's effectiveness for high-performance applications, showcasing excellent impedance matching, isolation, diversity, and gain characteristics. The overall mean percentage error between the measured and simulated results is -1.73%, with a standard deviation of 12.4%, indicating a high level of consistency between experimental and theoretical findings.

Table 2 Comparison of the measured and simulated results

Parameter	Impedance Bandwidth (GHz)	ECC	TARC (dB)	DG (dB)	Isolation (dB)	Gain (dB)
Simulated	2.76 – 4.72 5.20 – 5.52	<0.01	-38.52 -51.33	~9.99	>-30	5.10
Measured	2.66 – 3.76 5.40 – 5.56	<0.001	-39.66 -58.17	~9.99	>-25	5.06

5.Discussion

The designed MIMO antenna resonates at two frequency bands: 3.14 GHz and 5.42 GHz. As a dual-band antenna, it operates on two separate frequency ranges, allowing it to support different technologies or communication standards within the same device. This enhances the antenna's versatility, eliminating the need for multiple antennas to support different bands. 3.14 GHz is in the Sub-6 GHz band, which is commonly utilized in 5G NR to provide widespread, high-speed data delivery. This range offers a balance between faster data speeds and extended coverage. The 5.42 GHz frequency falls within the 5 GHz band, which is frequently used for Wi-Fi networks. With a shorter range, it provides greater data speeds than lower frequency bands like 2.4 GHz. With minimal mutual coupling and great spatial diversity, the measured and simulated ECC values are rather low, particularly in the critical bands (likely 3.14 GHz and 5.42 GHz), suggesting that the antenna system is performing well. The antenna demonstrates excellent impedance matching and efficiency across these bands, as indicated by reflection coefficients consistently below -10 dB at the two resonant frequencies. The measured isolation values follow the same trend as the simulated results, staying consistently below -20 dB across the frequency band. There is some slight variation in the measured data compared to the simulated results, but isolation remains well below -15 dB, even in the worst case. Low ECC maximizes system speed and reliability by ensuring that the antenna elements may broadcast and receive independent data streams. The overall performance remains strong, although a small discrepancy between the simulated and observed values occurs around 2.5 GHz. This difference can be attributed to real-world factors such as manufacturing tolerances, environment-induced coupling, or measurement errors. The MIMO antenna system demonstrates exceptional diversity performance, as reflected in the measured DG values, which consistently reach 10 dB. This ensures the system effectively mitigates signal fading, enabling more robust and reliable communication, particularly in challenging environments such as urban areas and indoor spaces. Minor variations in the simulated DG at 2.5 GHz align with a slight increase in ECC at this frequency, suggesting a marginal impact on diversity due to coupling effects or reduced isolation. However, overall diversity performance remains excellent across the operating frequency range.

Table 3 presents a performance comparison between the proposed antenna design and existing designs. The proposed antenna achieves superior isolation of -25.8 dB and -39.5 dB, low ECC (<0.001), and excellent TARC (<-50 dB), all while maintaining a compact footprint of 59 × 20 mm. These attributes establish its clear advantage in terms of diversity performance and compactness, making it highly suitable for 5G applications.

Table 3 Performance comparison between the proposed antenna design and existing designs

Ref. No.	No. of Ports	Freq. (GHz)	BW (GHz)	Isolation (dB)	ECC	TARC (dB)	DG	CCL	Size (mm)	Technique used
[35]	2	3.9, 5.2, 7.1, 9.1	-	>30	-	-	-	-	38×25	reduced ground, circular slot, rectangular slot
[36]	2	2.95–6.3	2.3	15	0.012	-10	10	0.05	20×34	ground stub
[37]	2	18.9–34.8	9.5	35	0.005	-10	9.99	0.2	26×26	self-isolation
[38]	2	3.12–5	-	16	0.025	-	-	-	25×20	parasitic ground stub
[39]	2	26.3 – 34	7.7	>25	0.0001	<-16	>9.9	>0.25	26×16	designed for high frequency using an array of two elements and implanted with a dual port
[40]	2	5.2-5.7	0.5	-20	<0.004	<−10	>9.9	-	30×30	DGS
[41]	2	3.25 – 5	1.75	>15	-	-	-	-	44×27	1 × 2 array of elliptical-shaped artificial metamaterial
This design	2	2.75 – 4.64 and 5.24 – 5.53	2.18	-25.8 and -39.5	<0.001	<-50	>9.9	<0.05	59×20	slotted antenna and DGS

The proposed MIMO antenna design achieves excellent isolation and broad bandwidth, yet some challenges remain. One significant concern is further miniaturization without affecting performance, as reducing size often leads to higher mutual coupling. Additionally, the use of FR4 material results in moderate dielectric losses, which may influence overall efficiency. Minor variations in fabrication and environmental conditions could also cause slight differences between simulated and measured results. While the antenna provides a satisfactory gain, further optimization is needed to enhance efficiency, particularly in high-frequency 5G applications. Moreover, since the current design primarily supports sub-6 GHz bands, future research should focus on expanding its functionality to cover multi-band or higher-frequency applications. A complete list of abbreviations is listed in *Appendix I*.

6.Conclusion and future work

An attempt was made to achieve the target frequency and enhance the MIMO antenna's performance by reducing its original size by half. The goal of this research was to design a compact, FR-4-based, dual-band MIMO antenna for use in the C-band. This study presented a highly isolated, compact, dual-band MIMO antenna designed for 5G network applications. The design achieves substantial bandwidth enhancement and isolation through the incorporation of triangular radiating elements, a rectangular isolation strip, and circular and rectangular slots. The antenna achieves isolation values of -25 dB and -42.59 dB, with an ECC of 0.001, at resonant frequencies of 3.14 GHz and 5.42 GHz, respectively. The measured results closely align with the simulations, confirming the design's suitability for 5G C-band applications, delivering reliable performance, minimal mutual coupling, and high DG. Although the design achieves good isolation and performance, challenges remain in further miniaturizing the antenna and enhancing its gain. The primary limitations of this research include challenges in further miniaturizing the antenna while maintaining high performance and the moderate losses associated with the use of FR-4 material, which can affect efficiency. Future research should focus on enhancing antenna gain using techniques like AMC integration and substrate-integrated waveguide (SIW) cavities. They should also explore advanced materials with lower loss and higher performance to achieve further improvements. Additionally, designing multi-band antennas with enhanced compactness and isolation for next-generation 5G and 6G systems can expand the design's applicability across a wider range of applications.

Acknowledgment
None.

Conflicts of interest
The authors have no conflicts of interest to declare.

Data availability
None.

Author's contribution statement
Kakade Sandeep: Conceptualization, investigation, design, draft manuscript preparation, review and editing.
Dr. Nirmal Sharma- Supervision, investigation on challenges and analysis. **Dr. Navnath Narawade-** Supervision, investigation on challenges and analysis.

References
[1] Tran HH, Nguyen TT, Ta HN, Pham DP. A metasurface-based MIMO antenna with compact, wideband, and high isolation characteristics for sub-6 GHz 5G applications. IEEE Access. 2023; 11:67737-44.
[2] Güler C, Bayer KSE. A novel high isolation 4-port compact MIMO antenna with DGS for 5G applications. Micromachines. 2023; 14(7):1-17.
[3] Singh A, Kumar A, Kanaujia BK. High gain and enhanced isolation MIMO antenna with FSS and metasurface. Optik. 2023; 286:170982.
[4] Raj T, Mishra R, Kumar P, Kapoor A. Advances in MIMO antenna design for 5G: avcomprehensive review. Sensors. 2023; 23(14):1-34.
[5] Aliqab K, Armghan A, Alsharari M, Aly MH. Highly decoupled and high gain conformal two-port MIMO antenna for V2X communications. Alexandria Engineering Journal. 2023; 74:599-610.
[6] Elalaouy O, El GM, Foshi J. Mutual coupling reduction of a two-port MIMO antenna using defected ground structure. e-Prime-Advances in Electrical Engineering, Electronics and Energy. 2024; 8:100557.
[7] Kiani SH, Munir ME, Savci HS, Rimli H, Alabdulkreem E, Elmannai H, et al. Dual-polarized wideband 5G N77 band slotted MIMO antenna system for next-generation smartphones. IEEE Access. 2024; 12:34467-76.
[8] Luadang B, Janpangngern P, Pookkapund K, Dentri S, Krairiksh M, Phongcharoenpanich C. Broadband unidirectional twin-element MIMO antenna scheme for mid-band 5G and WLAN laptops. Scientific Reports. 2024; 14(1):1-23.
[9] Roges R, Sharma S, Malik PK, Islam T, Asha S, Das S. A compact circularly polarized dual port MIMO antenna with DGS and parasitic patch for modern wireless communication and IOT applications. Physica Scripta. 2024; 99(5):055515.
[10] Rajavel V, Ghoshal D. Enhancement of off-body communications with a low-SAR, high-gain multiband patch antenna designed with a quad-band artificial magnetic conductor. International Journal of Microwave and Wireless Technologies. 2024; 16(2):318-38.
[11] Hamlbar GH, Kazemi R, Fathy AE. Development of a metasurface-based slot antenna for 5G MIMO applications with minimized cross-polarization and stable radiation patterns through mode manipulation. Scientific Reports. 2024; 14(1):1-18.
[12] Islam T, Alsaleem F, Alsunaydih FN, Alhassoon K. Mutual coupling reduction in compact MIMO antenna operating on 28 GHz by using novel decoupling structure. Micromachines. 2023; 14(11):1-12.
[13] Sharma S, Kumar M. Design and analysis of a 4-port MIMO microstrip patch antenna for 5G mid band applications. Progress In Electromagnetics Research. 2023; 129(2022):231-43.
[14] Kempanna SB, Biradar RC, Kumar P, Kumar P, Pathan S, Ali T. Characteristic-mode-analysis-based compact vase-shaped two-element uwb mimo antenna using a unique DGS for wireless communication. Journal of Sensor and Actuator Networks. 2023; 12(3):1-17.
[15] Saad H, Mosleh MF, Abd-alhameed R. Design a dual polarizations MIMO antenna based on decoupling elements for 5G smart-phones. Journal of Techniques. 2023; 5(1):74-85.
[16] Elechi P, John PR. Improved multiband rectangular microstrip patch antenna for 5G application. Journal of Telecommunication, Electronic and Computer Engineering (JTEC). 2022; 14(2):7-14.
[17] Sandi E, Diamah A, Al MM. High isolation MIMO antenna for 5G C-band application by using combination of dielectric resonator, electromagnetic bandgap, and defected ground structure. EURASIP Journal on Wireless Communications and Networking. 2022; 2022(1):1-13.
[18] Hasan MM, Islam MT, Samsuzzaman M, Baharuddin MH, Soliman MS, Alzamil A, et al. Gain and isolation enhancement of a wideband MIMO antenna using

metasurface for 5G sub-6 GHz communication systems. Scientific Reports. 2022; 12(1):1-17.
[19] Kaushal V, Birwal A, Patel K. Diversity characteristics of four-element ring slot-based MIMO antenna for sub-6-GHz applications. ETRI Journal. 2023; 45(4):581-93.
[20] Pallavi HV, Jagadeesh AP. Design and analysis of MIMO patch antenna for 5G wireless communication systems. International Journal of Computer Networks and Communications. 2022; 14(4):41-56.
[21] Kanagasabai M, Shanmuganathan S, Alsath MG, Palaniswamy SK. A novel low-profile 5G MIMO antenna for vehicular communication. International Journal of Antennas and Propagation. 2022; 2022(1):1-12.
[22] Ahmad A, Choi DY, Ullah S. A compact two elements MIMO antenna for 5G communication. Scientific Reports. 2022; 12(1):1-8.
[23] Emara HM, El DSK, Ghouz HH, Sree MA, Fatah SA. Compact high gain microstrip array antenna using DGS structure for 5G applications. Progress in Electromagnetics Research C. 2023; 130:213-25.
[24] Ranjan P, Yadav S, Bage A. Dual band MIMO antenna for LTE, 4G and sub–6 GHz 5G applications. Facta Universitatis, Series: Electronics and Energetics. 2023; 36(1):43-51.
[25] Rana S, Gautam AK, Sharma S, Batra R. A novel compact ultra-wide band MIMO antenna for WLAN 5G & sub-6GHz wireless applications. In international conference on computing, power and communication technologies 2024 (pp. 1159-64). IEEE.
[26] Salim N, Singh MS, Abed AT, Islam MT. 4X4 MIMO slot antenna spanner shaped low mutual coupling for Wi-Fi 6 and 5G communications. Alexandria Engineering Journal. 2023; 78:141-8.
[27] Aung MS, Hla TT. Two-port wideband MIMO antenna for sub-6GHz 5G applications. In IEEE conference on computer applications 2024 (pp. 1-6). IEEE.
[28] Iriqat S, Yenikaya S, Secmen M. Dual-band 2× 1 monopole antenna array and its MIMO configuration for WiMAX, sub-6 GHz, and sub-7 GHz applications. Electronics. 2024; 13(8):1-20.
[29] Ghosh S, Baghel GS, Swati MV. Design of a highly-isolated, high-gain, compact 4-port MIMO antenna loaded with CSRR and DGS for millimeter wave 5G communications. AEU-International Journal of Electronics and Communications. 2023; 169:154721.
[30] Das GS, Chamuah BB, Beria Y, Kalita PP, Buragohain A. Compact four elements SUB-6 GHz MIMO antenna for 5G applications. Materials Today: Proceedings. 2023.
[31] Madhumitha K, Prabhaa BR, Dharshanya P. Two element MIMO antenna design for wireless applications. In 2nd international conference on advancements in electrical, electronics, communication, computing and automation 2023 (pp. 1-5). IEEE.
[32] Khedr AA, Elnaghi BE, Mohamed AM. Design of a compact dual port 2 x 1 ultra-wideband MIMO antenna for radio frequency energy harvesting based on four" a" shaped slots. Progress in Electromagnetics Research M. 2024; 128:41-9.
[33] Jha P, Kumar A, De A. Two-port miniaturized textile antenna for 5G and WLAN applications. International Journal of Microwave and Wireless Technologies. 2023; 15(8):1443-52.
[34] Qin Y, Zhang L, Mao CX, Zhu H. A compact wideband antenna with suppressed mutual coupling for 5G MIMO applications. IEEE Antennas and Wireless Propagation Letters. 2022; 22(4):938-42.
[35] Kumar A, Pattanayak P, Verma RK, Sabat D, Prasad G. Two-element MIMO antenna system for multiband millimeter-wave, 5G mobile communication, Ka-band, and future 6G applications with SAR analysis. AEU-International Journal of Electronics and Communications. 2023; 171:154876.
[36] Gollamudi NK, Narayana YV, Prasad AM. Compact and asymmetric fed modified hexagonal shaped multiple-input multiple-output (MIMO) antenna for 5G sub: 6 GHz (N77/N78 & N79) and WLAN applications. Analog Integrated Circuits and Signal Processing. 2023; 114(1):103-12.
[37] Singh AK, Pandey A, Mishra PK, Yadav RS. A miniaturized 2× 2 double flare horn shaped mimo antenna with enhanced isolation for k and ka band applications. Progress In Electromagnetics Research M. 2022; 111:159-71.
[38] Kulkarni J, Gangwar RK, Anguera J. Broadband and compact circularly polarized MIMO antenna with concentric rings and oval slots for 5G application. IEEE Access. 2022; 10:29925-36.
[39] Raheel K, Ahmad AW, Khan S, Shah SA, Shah IA, Dalarsson M. Design and performance evaluation of orthogonally polarized corporate feed MIMO antenna array for next-generation communication system. IEEE Access. 2024; 12:30382-97.
[40] Ali A, Munir ME, Nasralla MM, Esmail MA, Al-gburi AJ, Bhatti FA. Design process of a compact tri-band MIMO antenna with wideband characteristics for sub-6 GHz, Ku-band, and millimeter-wave applications. Ain Shams Engineering Journal. 2024; 15(3):1-13.
[41] Singh G, Abrol A, Kumar S, Kanaujia BK, Pandey VK. Isolation enhancement in a two-element MIMO antenna using electromagnetic metamaterial. In international conference on device intelligence, computing and communication technologies 2023 (pp. 131-5). IEEE.

Mr. Kakade Sandeep earned his bachelor's degree in Electronics and Telecommunication Engineering in 2006 and his master's degree in 2013, both from Dr. Babasaheb Ambedkar Marathwada University, Aurangabad. He is currently pursuing a PhD in Electronics and Communication Engineering at the School of Engineering and Technology, Nirwan University, Jaipur, Rajasthan. To date, he has

published seven research papers in esteemed conferences and journals.
Email: kakadesandeep2000@gmail.com

Prof. (Dr.) Nirmal Sharma is a professor at the School of Engineering and Technology, Nirwan University, Jaipur. With over 20 years of experience as a senior research engineer and academician, she has successfully completed 44 research projects and published 26 research papers in reputed conferences and journals.
Email: drnirmalsharmaindian@gmail.com

Prof. (Dr.) Navnath Narawade has been serving as the principal of Parvatibai Genba Moze College of Engineering, Wagholi, since 2015. He earned his doctorate in 2015 from Sant Gadge Baba Amravati University, Amravati. With a remarkable academic career, he has published over 40 research papers in international journals and conferences, holds two patents, and has authored three books.
Email: nsnarawade@gmail.com

Appendix I

S. No.	Abbreviation	Description
1	4G	Fourth-Generation
2	5G	Fifth-Generation
3	6G	Sixth-Generation
4	AMC	Artificial Magnetic Conductors
5	CCL	Channel Capacity Loss
6	CSRR	Complementary Split-Ring Resonator
7	CST	Computer Simulation Technology
8	DG	Diversity Gain
9	DGS	Defected Ground Structure
10	ECC	Envelope Correlation Coefficient
11	FR4	Flame Retardant 4
12	HFSS	High Frequency Structure Simulator
13	IoT	Internet of Things
14	LTE	Long Term Evolution
15	MEG	Mean Effective Gain
16	MIMO	Multiple-Input-Multiple-Output
17	NR	New Radio
18	PEC	Perfect Electric Conductor
19	RF	Radio Frequency
20	SAR	Specific Absorption Rate
21	SIW	Substrate-Integrated Waveguide
22	SMA	Sub-Miniature Version A
23	TARC	Total Active Reflection Coefficient
24	UWB	Ultra-Wideband
25	VNA	Vector Network Analyzer
26	VSWR	Voltage Standing Wave Ratio